Kinetic roughening of electrodeposited films

2004 J. Phys.: Condens. Matter 16 R859

(http://iopscience.iop.org/0953-8984/16/26/R01)

INSTITUTE OF PHYSICS PUBLISHING JOURNAL OF PHYSICS: CONDENSED MATTER

J. Phys.: Condens. Matter **16** (2004) R859–R880 PII: S0953-8984(04)29858-7

TOPICAL REVIEW

Kinetic roughening of electrodeposited films

W Schwarzacher

H H Wills Physics Laboratory, Tyndall Avenue, Bristol BS8 1TL, UK

Received 24 March 2004
Published 18 June 2004
Online at stacks.iop.org/JPhysCM/16/R859
doi:10.1088/0953-8984/16/26/R01

Abstract

Recent work on the kinetic roughening of compact films electrodeposited on two-dimensional substrates is reviewed. We show how characteristic features of the electrodeposition process, in particular mass transport by bulk diffusion in the electrolyte, give rise to morphological instabilities, and present the results of their investigation by linear stability analysis. We then introduce power law descriptions of kinetic roughening and, after a brief discussion of theoretical treatments of electrodeposition incorporating scaling analysis, show that anomalous dynamic scaling describes many experimental results well. Results from Cu films electrodeposited in the absence and presence of organic additives are summarized, and attention is drawn to the possible relationship between the power law exponent β_{loc} (giving the time dependence of the small scale roughness) and the diffusional instability. Further results are presented from other systems including electrodeposited Ni, Ag and alloys, and the major experimental and theoretical challenges that remain are discussed.

Contents

1. Introduction

Kinetic roughening is a widely studied phenomenon that is of both fundamental interest and practical relevance [1, 2]. It occurs when material is added to or removed from a surface away from equilibrium, and occurs on length scales ranging from the atomic (in thin film deposition or dissolution, for example) to the macroscopic (e.g. in the build-up of sediments). In this article, we concentrate on one particular example of kinetic roughening, namely that which occurs when a metal film is prepared by electrochemical deposition, otherwise known as electrodeposition or electroplating, on a two-dimensional substrate. Furthermore, we shall concentrate on the growth of compact rather than ramified films, and pay particular attention to systems where the roughness appears to obey power laws.

2. Electrodeposition

2.1. Introduction

Electrodeposition is economically important because of its low cost and flexibility. It has the two particular advantages of not requiring a vacuum system and being a selective method, in the sense that deposition only takes place where there is a conducting path to the external circuit. Although electrodeposited films first found widespread application as decorative and/or protective coatings, electrodeposition is now also widely used in the electronics industry to deposit conducting or magnetic layers. For example, electrodeposited Cu is now the material of choice for the interconnects in ultra-large scale integrated (ULSI) circuits [3], while electrodeposited soft magnetic alloys are an important component of magnetic recording heads.

Figure 1 illustrates the basic principle of electrodeposition. Two conducting electrodes are placed in an electrolyte containing ions of the metal or metals to be deposited. When the external power supply drives a current through the cell, metal ions are reduced to metal atoms at one of the electrodes, known as the cathode. For example, if the electrolyte contained dissolved Cu^{2+} ions, the cathode reaction would be

$$Cu^{2+}_{(aqueous)} + 2e^- \rightarrow Cu_{(solid)}. \quad (1)$$

The cathode therefore forms the substrate of the electrodeposited film, and is also referred to as the working electrode. To complete the circuit, an oxidation reaction takes place at the second electrode, known as the anode or counter-electrode.

Electrodeposition is referred to as either ‘potentiostatic’ or ‘galvanostatic’, depending on whether the external power supply is used to fix the potential applied to the substrate or the current passing through it. For potentiostatic deposition it is usual to measure the working electrode (substrate) potential relative to an additional reference electrode. Very little current passes through the reference electrode, which does not become polarized and remains at a well defined potential, unlike the anode.

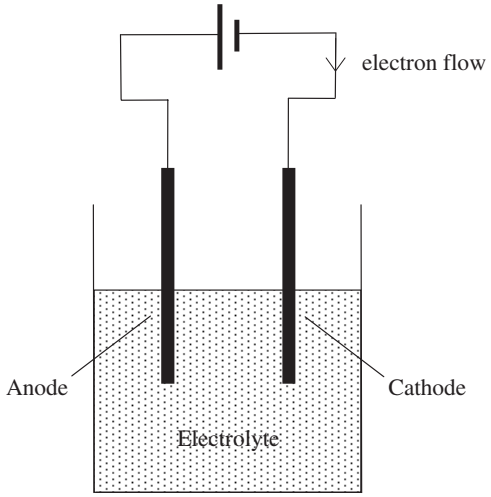

Figure 1. Schematic diagram of a simple electrodeposition cell.

2.2. Equilibrium potential and electrode kinetics

In addition to the deposition reaction, the reverse reaction (metal dissolution) generally also occurs at the working electrode. For example (1), this would be

$$\mathrm{Cu_{(solid)}} \rightarrow \mathrm{Cu^{2+}_{(aqueous)}} + 2\mathrm{e}^{-}. \tag{2}$$

If the cathode potential is made more negative then the rate of reaction (1) increases while that of reaction (2) decreases, while if the cathode potential is made more positive the opposite occurs. The potential at which the rates of the forward and reverse reactions (1) and (2) are equal is the equilibrium potential E_{eq}, which depends on the concentration of Cu^{2+} ions in the electrolyte (written as $[Cu^{2+}]$, which has units mol l^{-1}, written M).

For the generalized metal reduction reaction

$$\mathrm{M}^{n+} + n\mathrm{e}^{-} \leftrightarrow \mathrm{M}, \tag{3}$$

E_{eq} is given by the Nernst equation:

$$E_{\mathrm{eq}} = E^{0\prime} + \frac{kT}{ne} \ln[\mathrm{M}^{n+}], \tag{4}$$

where the constant $E^{0\prime}$ is the 'formal potential'. The rate of metal deposition is controlled by the overpotential η, given by $\eta = E_{\mathrm{eq}} - E$, where E is the potential applied to the working electrode. Note that when E is more negative than E_{eq}, favouring metal deposition, η is positive. Note also that to determine η for a given electrodeposition experiment it is not only necessary to know E but also $[\mathrm{M}^{n+}]$ at the working electrode, since the latter determines E_{eq} (equation (4)), but is not necessarily equal to the bulk concentration of M^{n+}.

Assuming that η is sufficiently positive that the rate of dissolution is negligible, the deposition current density j (which is equal to the rate of metal deposition per unit area multiplied by $-ne$) very often obeys a relationship of the form

$$j = -j_0[\mathrm{M}^{n+}]^{\gamma} \mathrm{e}^{\alpha ne\eta/kT} \tag{5}$$

where j_0 and α are positive constants. When (5) applies to a system, this is known as Tafel behaviour, and the higher the value of the constant j_0 the more facile is the electron transfer. By convention, reduction at the working electrode corresponds to a negative current. In the remainder of this review, we shall assume that the exponent γ in (5) is equal to one.

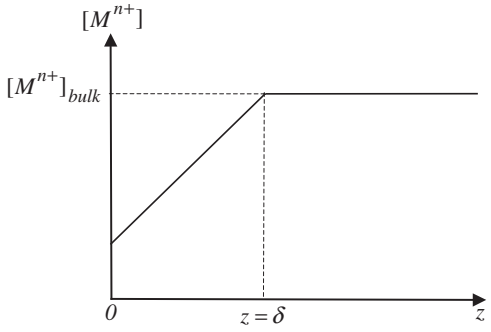

Figure 2. Schematic diagram of concentration profile close to cathode surface ($z = 0$).

Many processes other than the electron transfer described by equation (1) or similar can take place when electrodepositing a metal film. Some are common to electrodeposition and other thin film growth processes like sputtering or molecular beam epitaxy (MBE). These include the surface diffusion of ad-atoms and their incorporation at lattice sites. Other processes are peculiar to electrodeposition. From the point of view of kinetic roughening, probably the most important of these are the dissolution and re-deposition of metal atoms at the electrode surface, and the transport of ions to the electrode under influence of the electric field (electromigration), the concentration gradient (diffusion) and any induced flow of solvent molecules (convection). It is these differences between electrodeposition and other thin film growth methods that give rise to particularly interesting physics (though mass transport effects are also important e.g. in chemical vapour deposition).

3. Morphological instabilities in electrodeposition

3.1. Diffusion in the electrolyte

Close to the cathode where the metal electrodeposition reaction (3) is taking place, the electrolyte will be depleted of M^{n+}. However, forced convection (stirring), and/or natural convection, caused by variations in the electrolyte density associated with variations in the concentrations of dissolved species or in the temperature, usually ensure that at some distance δ from the cathode $[M^{n+}]$ has its bulk value. Consequently, to a first approximation, the concentration profile close to the cathode is as shown in figure 2. (In reality there will be no discontinuity in the M^{n+} concentration gradient $\frac{\partial}{\partial z}[M^{n+}]$.)

Within the layer of thickness δ next to the cathode, shown in figure 2, $\frac{\partial}{\partial z}[M^{n+}]$ is non-zero and diffusion therefore makes a significant contribution to the transport of M^{n+}. This layer is known as the diffusion layer. The diffusion flux F_D is given by Fick's first law,

$$F_D = -D\nabla[M^{n+}] = -D\frac{\partial}{\partial z}[M^{n+}] = -D\frac{[M^{n+}]_{bulk} - [M^{n+}]_{z=0}}{\delta}, \tag{6}$$

and the corresponding current density j_D by

$$j_D = -nFD\frac{[M^{n+}]_{bulk} - [M^{n+}]_{z=0}}{\delta}, \tag{7}$$

where F is Faraday's constant, the magnitude of the charge on 1 mol of electrons. Note that since $[M^{n+}]$ at the cathode cannot be less than zero, the magnitude of j_D has a maximum for

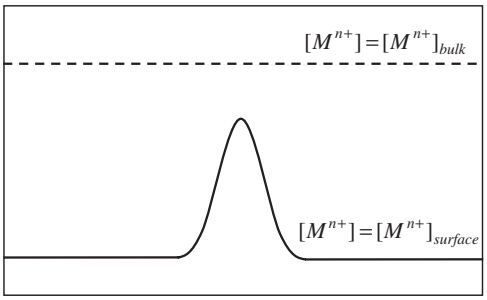

Figure 3. The concentration contours $[M^{n+}] = [M^{n+}]_{bulk}$ and $[M^{n+}] = [M^{n+}]_{surface}$ around a protuberance on the cathode.

j_{DL}, given by

$$j_{DL} = -\frac{nFD[M^{n+}]_{bulk}}{\delta}. \tag{8}$$

j_{DL} is known as the diffusion-limited current density.

Diffusion in the electrolyte can give rise to a morphological instability in the sense that any surface irregularities are amplified rather than damped during growth. This instability, which is closely related to the Mullins–Sekerka instability [4], is illustrated by figure 3, which shows the contours $[M^{n+}] = [M^{n+}]_{bulk}$ and $[M^{n+}] = [M^{n+}]_{surface}$ around a protuberance on the cathode. The intermediate contours will be most closely spaced, and the concentration gradient and consequently the diffusion flux will therefore be greatest near the tip of the protuberance. In general, points closer to the edge of the diffusion layer, where $[M^{n+}]$ has its bulk value, receive greater flux. In the situation shown in figure 3, since the rate at at which M^{n+} diffuses to the cathode increases towards the tip of the protrusion, so too does the rate of M deposition. Hence diffusion can cause peaks on the cathode surface to grow more rapidly than valleys, amplifying any pre-existing roughness.

3.2. Other destabilizing and stabilizing influences

If electromigration were to dominate mass transport close to the surface, then this would also have a destabilizing effect, since, like the contours of constant $[M^{n+}]$, the contours of constant electrostatic potential will be most closely spaced and the electric field correspondingly greatest near the tips of a protuberance. When both electromigration and diffusion are important, the situation is more complicated. It is, however, possible to minimize the influence of electromigration by the addition of so-called supporting electrolyte. The ions of the supporting electrolyte do not take part in the electrodeposition reaction, but move in response to any electric field to equalize the electrostatic potential, eliminate the field and thereby remove the driving force for electromigration. An example of a supporting electrolyte would be sulfuric acid H_2SO_4 added to $CuSO_4$ for Cu electrodeposition. The H^+ ions are highly mobile, and therefore perform the role of supporting electrolyte effectively.

The electrode kinetics reduce the destabilizing effect of diffusion in the electrolyte, because, from (5), if the applied potential E is fixed, any local increase in current density e.g. at the tip of a protuberance requires an increase in $[M^{n+}]$. Raising the overpotential η is only possible if the equilibrium potential E_{eq} becomes more positive. However, from (4) a more positive E_{eq} requires a higher $[M^{n+}]$. The increase in $[M^{n+}]$ reduces the change in

$[M^{n+}]$ between the edge of the diffusion layer and the electrode, reducing the driving force for diffusion and consequently the diffusion flux to the protuberance.

Surface tension gives rise to an additional term in the electrochemical potential at the surface. Where the curvature is negative (i.e. at protuberances), this term reduces η, reducing the rate of deposition and increasing the rate of dissolution. As well as modifying the local rate of deposition/dissolution, the surface tension also opposes surface roughening by driving surface diffusion (as distinct from bulk diffusion in the electrolyte) from regions of negative curvature to regions of positive curvature.

3.3. The role of additives

In addition to the M^{n+} ions, many electrolytes contain components that influence the electrodeposition reaction by adsorbing on the electrode surface. These additional components are given the general name additives. The simplest additives are the anions which must be present in the electrolyte to ensure electrical neutrality. Different anions adsorb on the electrode surface with different strengths at different potentials. Cl^- anions play a particularly important role in Cu electrodeposition on Cu(100), for example, because they can form an ordered adlayer on the Cu surface, which gives a preferred step orientation parallel to [010] and [001] [5, 6]. The adsorbed Cl^- profoundly affects the morphology of the electrodeposited Cu, giving rise to features with fourfold symmetry such as pyramidal mounds and blocks [7, 8].

Organic molecules are also widely used as additives. Many suggestions have been made as to how they influence the morphology of electrodeposited films [9], but the most common proposed mechanism is that by adsorbing on the surface they block lattice sites. This either affects the growth directly, by preventing the incorporation of M atoms at these sites, or indirectly, by inhibiting surface diffusion [10]. The influence of a blocking additive will also depend on whether it blocks specific sites preferentially, such as kink or step sites, or adsorbs at random locations.

Surface smoothening through additives is generally referred to as 'levelling' or 'brightening' in the electrodeposition literature, with the former generally referring to smoothening at much larger length scales than the latter. One simple explanation of levelling is that the additive diffuses more rapidly to peaks than to troughs, and therefore preferentially inhibits growth at the former. This process has been modelled e.g. by Madore *et al* who assumed that the additive coverage is proportional to the rate of additive consumption, which in turn is equal to the diffusive flux of additive [11].

Many commercially important electrolytes contain more than one additive, and in such cases the interactions between additives become important. The electrolytes used to deposit Cu for ULSI interconnects form a particularly interesting example [3]. In this application, Cu is deposited on a conducting substrate incorporating deep trenches and vias, and fills these preferentially, as shown in figure 4. This behaviour is known as superconformal filling and may be explained because the electrolyte contains additives that inhibit growth together with an additive that counteracts the inhibition (the 'accelerator'). According to the curvature enhanced accelerator coverage (CEAC) model, the growth rate is controlled by the coverage of the latter [12, 13]. Consider the example of figure 4. The accelerator coverage on the seed layer is initially uniform (figure 4(a)), but as growth continues the surface area inside the trench decreases, concentrating the accelerator (figure 4(b)), leading to rapid growth, which concentrates the accelerator still further (figure 4(c)), and leads eventually to a bump forming over the trench (figure 4(d)). The CEAC model enables accurate quantitative predictions of super-filling.

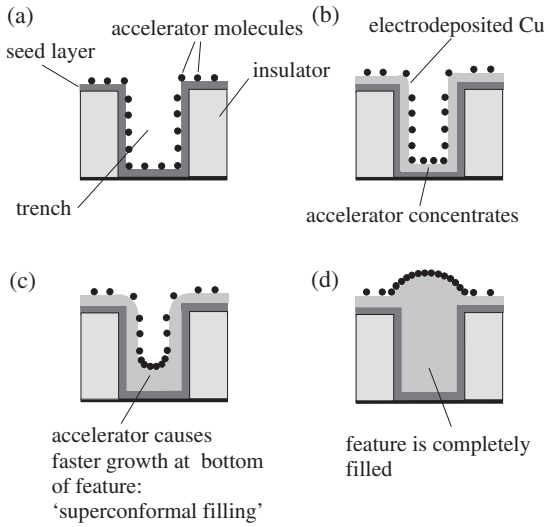

Figure 4. Schematic diagram showing superconformal filling according to the curvature enhanced accelerator coverage model. (a)–(d) represent successive stages of the deposition process.

4. Linear stability analysis

Linear stability analysis is a well established method of investigating the net effect of various competing influences on the surface morphology. Assuming the electrode surface to be parallel to the x–y plane, it involves calculating the response of the system to a small amplitude sinusoidal perturbation with wavevector $k_x\mathbf{i} + k_y\mathbf{j}$.

Aogaki and co-workers used linear stability analysis to study the competing influence of the diffusional instability and surface tension during potentiostatic electrodeposition [14]. They assumed constant electrical conductivity, and calculated the growth time constant p as a function of the wavelength $\lambda = 2\pi/k$ of the cathode perturbation ζ, given by

$$\zeta = \zeta_0 \exp[\mathrm{i}(k_x x + k_y y) + pt], \tag{9}$$

where the cathode is the surface $z = Z + \zeta$ with Z a constant, and t represents the deposition time. Surface tension effects were modelled through a surface potential $\phi(x, y, t)$, which modified the local deposition and dissolution rates.

$$\phi \propto -\left(\frac{\partial^2\zeta}{\partial x^2} + \frac{\partial^2\zeta}{\partial y^2}\right). \tag{10}$$

Positive values of p correspond to unstable growth, as perturbations grow in amplitude, while negative values of p correspond to stable growth.

To a good approximation, p can be written as the sum of a positive term proportional to $1/\lambda$ that is due to diffusion, and a negative term proportional to $1/\lambda^3$ that is due to surface tension. There is a critical wavelength λ_c below which the surface tension dominates and p is negative, and above which diffusion dominates and p is positive. p also has a maximum value $p_{\max}$ for some wavelength $\lambda_{\max}$. The dependence of p on λ is shown schematically in figure 5.

Aogaki and Makino carried out a similar linear stability analysis of galvanostatic deposition [15], and subsequently extended this work [16] to include a term describing surface diffusion driven by variations in the surface tension:

$$\left.\frac{\partial\zeta}{\partial t}\right|_{\text{surface diffusion}} \propto \nabla\cdot(\nabla\phi) \propto -\nabla^2(\nabla^2\zeta). \tag{11}$$

Note that the same term appears in kinetic roughening models that apply to molecular beam epitaxy, for example [17]. The surface diffusion term (11) gives a negative contribution to p proportional to $1/\lambda^4$. Hence it further suppresses the growth instability, as expected for a surface tension driven process.

Subsequently, Barkey and co-workers used linear stability analysis to show explicitly that electrode kinetics reduce the destabilizing effect of diffusion in the electrolyte [18], although, unlike the later work of Aogaki and Makino, they did not include surface diffusion driven by surface tension variations in their model. Chen and Jorne carried out a similar analysis [19], using equation (5) to describe the electrode kinetics, and allowing perturbation of the edge of the diffusion layer when $\delta \ll \lambda$. Despite the additional factors considered, qualitatively the results are very similar to figure 5: there is still a critical wavelength λ_c below which the surface is stable, and a wavelength λ_{max} for which the instability growth time constant has a maximum.

Others have also addressed this problem, the most recent being Haataja and co-workers, who investigated the role of the supporting electrolyte [20]. They found that while the dependence of p on λ again remained qualitatively as in figure 5, increasing the concentration of supporting electrolyte at fixed current density increased p_{max} and decreased λ_c, a result consistent with [19].

Haataja and co-workers also modelled the effects of additives on the linear stability [21], assuming

(i) that the additives interfere with the deposition process by blocking surface growth sites,
(ii) that the additives form complexes with the M^{n+} ions and therefore diffuse to regions where $[M^{n+}]$ is high and
(iii) that polar additives accumulate in regions with large electric fields.

Again, the results remain qualitatively as in figure 5, though the surface is stabilized if the bulk concentration of additives, their tendency to segregate onto the surface or form complexes, their dipole moment, or their rate of consumption is increased. Increasing any of these quantities can increase the additive coverage at protuberances relative to depressions, which, as in the levelling models mentioned earlier, suppresses growth at the former.

McFadden *et al* applied linear stability analysis to a system where the CEAC model applies [22]. This was the first application of the CEAC model to growth on an initially smooth surface rather than in the sort of feature (typical depth $\sim$0.5 μm) shown in figure 4. They found that there is an optimum value of the accelerator concentration in the electrolyte that maximizes λ_c. The accelerator stabilizes the surface because it is diluted at protuberances and concentrated in depressions, by the same mechanism that is shown in figure 4. This is an important result, because it suggests that the CEAC model provides an explanation of brightening.

There have been attempts to model the morphology of a rough surface as a function of deposition time by allowing its Fourier components with different k to grow independently with the time constants $p(k)$ obtained from linear stability analysis [18, 23]. However, the growth of the different Fourier components is only independent when their amplitude is small. If the assumption that different Fourier components grow independently were correct, a dependence of p on λ as shown in figure 5 suggests that at sufficiently long times a constant characteristic length scale corresponding to the wavelength λ_{max} for which the instability growth time constant has a maximum would emerge. Experimentally, though, while a characteristic length scale is indeed observed, this tends to increase according to a power law rather than tend to a constant value. The use of power laws to describe kinetic roughening is discussed in detail in the following section.

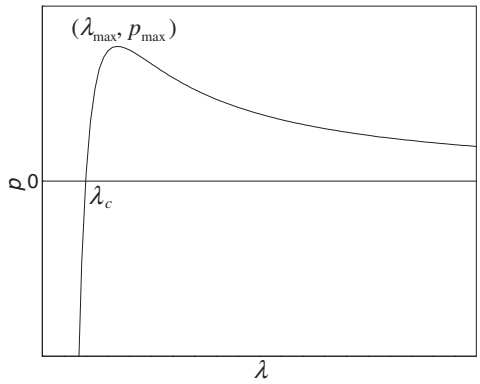

Figure 5. Schematic plot showing dependence of growth time constant p on perturbation wavelength λ according to linear stability analysis.

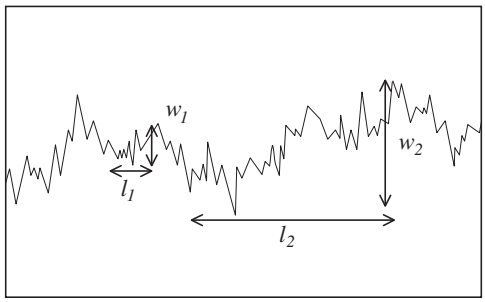

Figure 6. Schematic drawing of a rough surface.

5. Dynamic scaling analysis

5.1. Normal scaling

Any quantitative description of kinetic roughening must recognize that 'roughness' is a quantity that depends on the length scale on which it is observed. Figure 6 illustrates this point, since observing the roughness on length scale l_1 would give a value of the order of w_1, while observing it on length scale l_2 would give a value of the order of w_2. The scale-dependent quantity most often used as an experimental measure of roughness is the root-mean-square (rms) surface width $w(l)$, defined as

$$w(l) = \sqrt{\langle (h - \langle h \rangle)^2 \rangle} \tag{12}$$

where h is the surface height, and l is the size of the region over which w is measured. To study kinetic roughening, it is necessary to monitor this quantity as a function of t, which from now on we take to be the average film thickness rather than the deposition time, though the former is proportional to the latter for constant deposition rate. The thickness-dependent rms surface width is denoted by $w(l, t)$.

Normal (Family–Vicsek) dynamic scaling [24] postulates that $w(l, t)$ takes the following form:

$$w(l, t) \propto l^H \qquad \text{for } l \ll l_c \tag{13a}$$

$$w(l, t) \propto t^\beta \qquad \text{for } l \gg l_c \tag{13b}$$

where

$$l_c \propto t^{1/z}. \tag{14}$$

For consistency

$$z = H/\beta. \tag{15}$$

Normal scaling is illustrated in figure 7. For fixed t, $\log w \propto \log l$ below some value $l_c(t)$ and saturates above, taking a value which may be written as $w_{sat}(t)$. Note how l_c increases with t. Physically, $l_c(t)$ may be interpreted as the maximum length scale over which correlations in h are significant (correlation length), and $w_{sat}(t)$ as the long-range roughness.

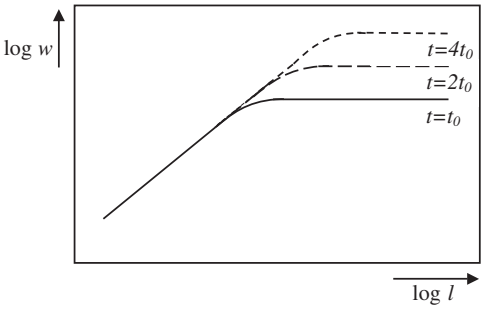

Figure 7. Root-mean-square surface width $w(l)$ at different values of the average film thickness t for a system exhibiting normal scaling.

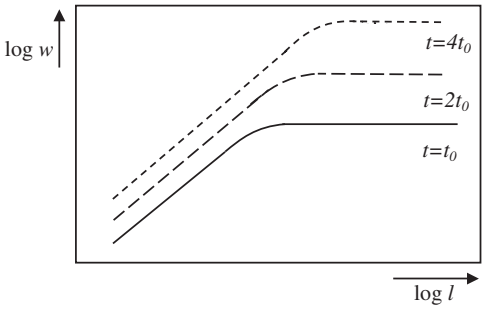

Figure 8. Root-mean-square surface width $w(l)$ at different values of the average film thickness t for a system exhibiting anomalous scaling.

Normal scaling was first observed in Monte Carlo simulations of ballistic deposition in (1 + 1) dimensions (i.e. one-dimensional substrate plus one growth dimension) [24]. It was also observed for models described by continuum equations [25]. Experimentally, low energy electron diffraction studies of Fe deposited on Fe(001) [26], and scanning tunnelling microscope (STM) studies of Ag evaporated on quartz [27], have shown normal scaling.

An alternative to working with $w(l)$ is to use the height–height correlation function $G(l)$:

$$G(l) = \sqrt{\left\langle (h(\mathbf{r}+\mathbf{l}) - h(\mathbf{r}))^2 \right\rangle} \tag{16}$$

where $|\mathbf{l}| = l$. The definition of $G(l)$ may be generalized as follows:

$$G_q(l) = \sqrt[q]{\left\langle |h(\mathbf{r}+\mathbf{l}) - h(\mathbf{r})|^q \right\rangle}. \tag{17}$$

If $G_q(l) \propto l^{H_q}$ for a range of l, and $H_q = H$ for all (positive) q, then in this length-scale range the surface is statistically self-affine with Hurst exponent H and local 'box counting' fractal dimension 3-H [1]. For a statistically self-affine surface with $G(l) \propto l^H$, $w(l) \propto l^H$ is also true. Note that for the special case of a planar surface $H = 1$. If H_q depends on q, the surface is multi-affine rather than simply self-affine [28].

5.2. Anomalous scaling

Equations (13)–(15) represent perhaps the simplest plausible power law behaviour that $w(l, t)$ could exhibit. However, more complex behaviour is also possible, and a number of model systems were found to obey the following scaling relationship [29, 30]:

$$w(l, t) \propto l^H \mathrm{t}^{\beta_{\mathrm{loc}}} \qquad \text{for } l \ll l_{\mathrm{c}} \tag{18a}$$

$$w(l, t) \propto t^{\beta+\beta_{\mathrm{loc}}} \qquad \text{for } l \gg l_{\mathrm{c}}. \tag{18b}$$

Equations (14) and (15) continue to apply. This type of scaling is known as anomalous scaling, and is illustrated in figure 8.

Comparison of equations (13) and (18) shows that normal scaling is the special case of anomalous scaling with $\beta_{\mathrm{loc}} = 0$. Equations (14), (15) and (18b) imply that w_{sat} and l_{c} are related by a power law:

$$w_{\mathrm{sat}} \propto {l_{\mathrm{c}}}^{\alpha} \tag{19}$$

where

$$\alpha = H(1 + \beta_{\mathrm{loc}}/\beta); \tag{20}$$

α is known as the roughness exponent. For normal scaling, α is equal to H because $\beta_{\mathrm{loc}} = 0$, but for anomalous scaling the distinction is important [31].

Clear evidence for anomalous scaling was obtained for Ag films evaporated on quartz, with interruptions to the growth to prevent sample heating [32]. Subsequently, a number of (1 + 1)-dimensional systems were found to exhibit such scaling, including cultivated brain tumours [33] and cracks in stone [34] and wood [35]. Anomalous scaling was also found in other (2+1)-dimensional systems, including polymer films prepared by vapour deposition [36].

5.3. Theoretical treatments of electrodeposition incorporating scaling analysis

In order to exhibit power law behaviour as described by equations (13) or (18), a model system must include some stochastic component. A fully deterministic system can show power law behaviour when the initial surface height distribution is chosen at random [37]. More usually, the rules governing the evolution of the surface height contain a stochastic component, as in equation (21)

$$\frac{\partial \zeta}{\partial t} = \nu \nabla^2 \zeta + \xi(\mathbf{r}, t) \tag{21}$$

where $\zeta = h(\mathbf{r}, t) - \langle h \rangle$ and $\mathbf{r} = x\mathbf{i} + y\mathbf{j}$ is the position vector of a point on a projection of the surface along the growth direction. Equation (21) describes the Edwards–Wilkinson model for kinetic roughening [38] in (2 + 1) dimensions. The same model in (1 + 1) dimensions ($\mathbf{r} = x\mathbf{i}$) gives normal scaling, and is perhaps the simplest model to do so. In equation (21), the first term on the right-hand side is a smoothing term that gives additional deposition where the surface curvature is positive, implying that the surface potential is lower than its mean value (see equation (10)), while $\xi(\mathbf{r}, t)$ represents the zero-mean, random fluctuation in the deposition flux. For the Edwards–Wilkinson model in $(d + 1)$ dimensions, $H = (2 - d)/2$ and $\beta = (2 - d)/4$.

Note that the Edwards–Wilkinson model is a local model, i.e. $\partial\zeta/\partial t\,(\mathbf{r}, t)$ does not depend on ζ at any other point $\mathbf{r}'$. Electrodeposition, however, is a non-local process, because the rate of diffusion of M^{n+} to $\mathbf{r}$ depends not only on $h(\mathbf{r}, t)$, but also on the heights at all the other points $\mathbf{r}'$. Even when diffusion in the electrolyte is significant, some authors have used local models to gain insight into kinetic roughening during electrodeposition [39]. For example, Buceta *et al* have studied the scaling properties of the stochastic stabilized Kuramoto–Sivashinsky equation in (1 + 1) dimensions [40, 41]:

$$\frac{\partial \zeta}{\partial t} = -\varepsilon\zeta - \nu\frac{\partial^2 \zeta}{\partial x^2} - \mu\frac{\partial^4 \zeta}{\partial x^4} + \frac{\lambda}{2}\left(\frac{\partial \zeta}{\partial x}\right)^2 + \xi(x, t). \tag{22}$$

The first term on the right-hand side of equation (2) is a stabilizing term, the second term is a destabilizing term favouring deposition at protrusions where the curvature is negative, the third term can represent surface diffusion (see equation (11)) and the fourth term represents the effect of growth occurring in a direction locally normal to the interface rather than in the z-direction [25]. As is found for electrodeposition (section 4 and figure 5), for equation (22) with appropriate choice of the constants ε, μ and ν, the growth is unstable for wavelengths above a critical wavelength λ_c. However, for the instability in equation (22), the growth time constant p contains terms proportional to $1/\lambda^2$ and $-1/\lambda^4$, whereas p for electrodeposition contains terms proportional to $1/\lambda$ and $-1/\lambda^3$.

Even though non-local models are computationally more intensive, a number of groups have studied their scaling properties. Sánchez and co-workers developed a non-local kinetic Monte Carlo model of electrodeposition which they named multiparticle biased diffusion limited aggregation (MBDLA) [42–44]. In MBDLA, a finite number of random walkers are

placed on a lattice to represent ions in an electrolyte, and a bias parameter is introduced to make motion in the direction of the electrode more probable than motion parallel to it. When a particle makes contact with the electrode, it sticks with a probability that is another of the model's parameters. The model may also be modified to incorporate surface diffusion [44]. Although the deposits generated by this model are, in general, non-compact, with voids and overhangs, a single-valued function $h(x, t)$ may still be defined as the height of the topmost particle belonging to the aggregate for column x at a particular stage t of the simulation. For a certain range of t, $h(x, t)$ was reported to exhibit anomalous scaling, and these authors were the first to suggest that electrodeposition would be a good technique with which to look for experimental evidence of such scaling [43].

More recently, De Leon *et al* modelled compact metal electrodeposition with a simpler (1+1)-dimensional kinetic Monte Carlo model where the probability that a metal atom attaches to the lattice site at x is proportional to $(h(x, t) - h_b(t))^{\delta_c}$, where $h_b(t)$ is the minimum value of h across all the sites and δ_c is an exponent [45]. The dependence on $h_b(t)$ means that this model is also non-local. After attachment, metal atoms are allowed to diffuse on the surface to maximize the number of nearest neighbours. Despite its simplicity, the model does incorporate some of the effects of diffusion in the electrolyte, as attachment to a peak is more probable than attachment in a valley, and the increasing importance of these effects as the current density approaches the diffusion-limited value j_{DL} may be represented by increasing δ_c. The model was also modified to incorporate the blocking effects of additives. The scaling properties of this model reported by de Leon *et al* are in very good agreement with experimental data for Cu deposition. This will be discussed in the next section.

6. Kinetic roughening and scaling of electrodeposited Cu films

6.1. Cu electrodeposition from organic additive-free electrolytes

Early experiments on the kinetic roughening of compact Cu electrodeposits considered (1+1)-dimensional growth from concentrated (0.5–2.0 M) $CuSO_4$ solutions in the absence of supporting electrolyte [46, 47]. These experiments were carried out in quasi-two-dimensional cells containing a thin (10–25 μm) layer of electrolyte between transparent plates, through which the morphology of the deposit could be monitored by optical microscopy. Kahanda *et al* observed the formation of a columnar structure, with deep crevices, and found that the growth time constant $p(k)$ for the Fourier component $h(k, t)$ of the measured interface profile $h(x, t)$ was in reasonable quantitative agreement with this structure being caused by the Mullins–Sekerka instability associated with electromigration [46]. This agreement may be fortuitous, given that both electromigration and diffusion should make a significant contribution to mass transport in this experiment, and given that the Mullins–Sekerka prediction applies to the case where the amplitudes of the different Fourier components are sufficiently small that their growth is independent, which would not appear to be the case here. The emergence and evolution of columnar structure associated with the mass transport instability is of considerable interest, and deserves additional study. It can best be studied in the (1 + 1)-dimensional geometry, because high aspect-ratio columns would be hard to measure on a two-dimensional substrate.

Nevertheless, studies of compact electrodeposition on two-dimensional substrates are extremely important, both because of their relevance to practical electroplating, and because it is possible to obtain surface profiles $h(\mathbf{r}, t)$ with extremely high resolution using scanning probe microscopy. This was demonstrated convincingly by Iwamoto and co-workers [48], who used atomic force microscopy (AFM) to measure the roughness of Cu films electrodeposited for different times from a stirred acid sulfate electrolyte (0.3 M $CuSO_4$/1.2 M H_2SO_4). Figure 9

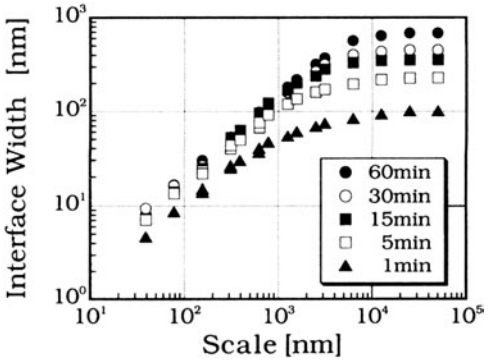

Figure 9. The interface width of Cu electrodeposits $w(l, t)$ versus length scale l for electrodeposition times of 1, 5, 15, 30 and 60 min. Figure reprinted with permission from [48]. © 1994 American Physical Society.

shows $w(l, t)$ calculated from AFM data for a series of films grown using a constant current density of 24 mA cm^{-2}, corresponding to a deposition rate of approximately 0.5 μm min^{-1}. For each of the films, ln $w(l)$ is proportional to ln l, and $w(l)$ saturates above some value l_c. ln $w_{sat}(t)$, the saturation value of w for a given film thickness, was also proportional to ln t. This work provided perhaps the first clear evidence for spatial and temporal power law behaviour in the kinetic roughening of electrodeposited films on a two-dimensional substrate.

A close comparison of figure 9 with figures 7 and 8 suggests that the data of Iwasaki *et al* might better be described by anomalous scaling than by normal scaling, at least for shorter deposition times. Clear evidence for anomalous scaling was found by Huo and Schwarzacher [49], who measured the scaling exponents H, β and β_{loc} (equations (18)) for a series of Cu films deposited at different current densities, on different substrates and from unstirred acid sulfate electrolytes with different [Cu^{2+}]. Their electrolyte and, probably, the other acid sulfate electrolytes referred to in this section contained trace Cl^-, which can have a strong influence on Cu electrodeposition even when present in sub-1 mM quantities. They obtained height data from their films by AFM with a resolution of 256 × 256 pixels, and subtracted a planar background to compensate for any tilt of the sample relative to the scanning plane. $w(l, t)$ was calculated by applying equation (12) to all square regions of side l in a particular image. Note that if the chosen region size contains too few data points, artefacts may be introduced due to the discrete nature of the surface sampling, and in this work l was always more than three times the dimension of a single image pixel.

Figure 10(a) shows a typical AFM image of a $t \approx 0.5$ μm Cu film electrodeposited from a 0.3 M $CuSO_4$/1.2 M H_2SO_4 electrolyte on a sputtered Cu (25 nm)/Ti (5 nm)/glass substrate. Figure 10(b) shows $w(l, t)$ plotted as a function of t for two different values of l, one satisfying $l \ll l_c$, and the other $l \gg l_c$. Note that in both cases ln $w(l, t)$ increases linearly with ln t. The slope of the log–log plot is β_{loc} for $l \ll l_c$, and $\beta + \beta_{loc}$ for $l \gg l_c$. Since both are clearly non-zero, the scaling is anomalous and equations (18) rather than (13) apply to these data.

Huo and Schwarzacher found that $\beta = 0.38 \pm 0.03$ and $H = 0.77 \pm 0.02$ remained constant independent of the deposition current density j, bulk electrolyte concentration [Cu^{2+}]$_{bulk}$, and whether Cu or Au substrates were used. Hence $\beta/H = 0.49 \pm 0.04$ is also constant and the correlation length l_c grows as $t^{\beta/H} = t^{0.49}$ (equations (14) and (15)) independent of the deposition conditions.

In contrast to H and β, β_{loc} could be varied by changing either the current density or the electrolyte concentration and appears to be a function of the ratio of the current to its diffusion-

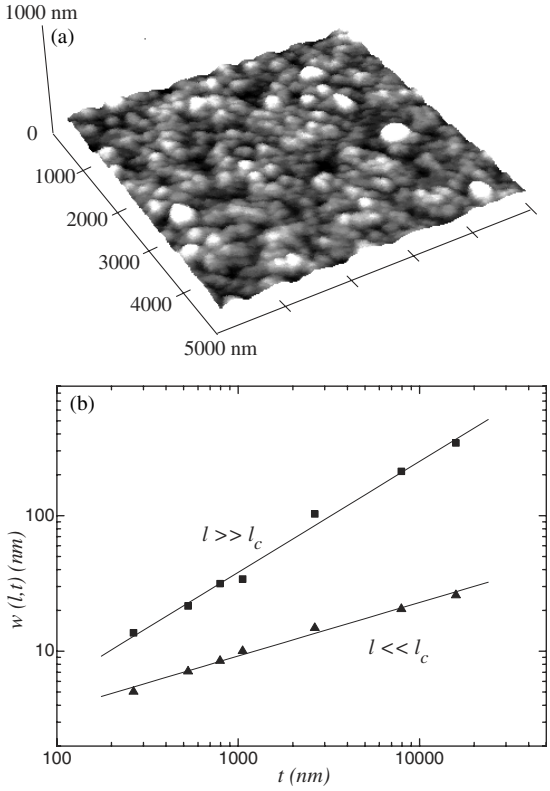

Figure 10. (a) AFM image of a $t \approx 0.5$ μm Cu film electrodeposited from a 0.3 M $CuSO_4$/1.2 M H_2SO_4 electrolyte on a sputtered Cu (25 nm)/Ti (5 nm)/glass substrate. (b) Surface width $w(l, t)$ for $l \ll l_c$ ($l = 100$ nm) and for $l \gg l_c$ measured from a series of Cu films of different thickness t deposited under the conditions of (a).

limited value j_{DL}, which the authors measured. As this ratio j/j_{DL} increases, β_{loc} increases from approximately 0 to 0.4. Using equation (18*b*), $w_{sat} \propto t^{\beta+\beta_{loc}}$, the maximum surface roughness w_{sat} grows as $t^{0.38}$ for the smallest values of β_{loc}, and as $t^{0.78}$ for the largest. Since w_{sat} grows as $t^{1/2}$ for purely random deposition (Poisson distribution), as j/j_{DL} increases, the kinetic roughening therefore changes from slower than in random deposition to faster, suggesting that growth is initially stabilized by the surface tension, but increasingly destabilized as a result of the diffusional instability.

Although this interpretation is intuitively appealing, it is possible that the instability causing the increase in β_{loc} is associated with an increase in the overpotential η rather than directly with the diffusional instability, because equations (5), (7) and (8) imply that η is also a function of j/j_{DL} when D and δ are constant (and assuming $j = j_D$). The increase in η could reduce the distance that adatoms can move before being incorporated in the growing film, for example, something that has been shown to cause β_{loc} to increase in one-dimensional simulations [29]. Increasing η is also likely to increase the rate of crystallite nucleation and give a finer-grained film. This may be one reason why w_{sat} with $t \approx 0.5$ μm was greater for films grown from the same electrolyte at lower current density and lower η [49], though the fact that $\beta + \beta_{loc}$ increases with increasing current density means that w_{sat} for a higher current density will exceed w_{sat} for a lower at some t.

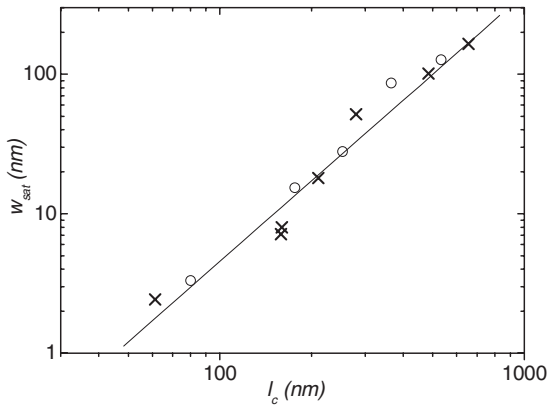

Figure 11. Logarithmic plot of w_{sat} as a function l_{c} for the centre (×) and edge (○) regions of Cu films of different thicknesses electrodeposited on a 60 μm diameter microelectrode from a 0.005 M $CuSO_4$/0.5 M H_2SO_4 electrolyte. The straight line is a fit to the data, and its slope gives the roughness exponent $\alpha = 1.9 \pm 0.2$ [50].

To distinguish between the diffusional instability and η as the cause of increasing β_{loc}, experiments are needed with varying D or δ. Preliminary measurements of this type do favour the diffusional instability, however, and non-electrochemical systems in which bulk diffusion plays a role also show evidence for anomalous scaling [36].

De Leon *et al* have published experimental data that confirms the dependence of $\beta + \beta_{\mathrm{loc}}$ on j/j_{DL} [45]. They are also able to reproduce this dependence using the simple model described in (5.3), taking the exponent $\delta_{\mathrm{c}} = j/j_{\mathrm{DL}}$. However, the authors do not report separate values for H, β and β_{loc}, and their model is $(1 + 1)$ dimensional, so further investigation is necessary to confirm the significance of the agreement between experiment and model.

Cecchini *et al* studied the kinetic roughening of Cu electrodeposited from 0.005 M $CuSO_4$/0.5 M H_2SO_4 on microelectrodes of diameter 60 μm formed by patterning a layer of photoresist on a Au (25 nm)/Ti (5 nm)/glass substrate [50]. Since mass transport to the centre of the microelectrode is controlled by planar diffusion, and that to the edge is more spherical, the current distribution is extremely non-uniform, and both the film thickness and w_{sat} were greater at the edge than centre. However, although j_{DL} varies across the microelectrode, the deposition potential was sufficiently negative that j was expected to be close to j_{DL} everywhere. This is likely to be the reason that β_{loc} was found to be the same in the centre and at the edge, and very close to the values measured by Huo and Schwarzacher for j close to j_{DL}. The measured values of $H = 0.84 \pm 0.02$ and $\beta = 0.36 \pm 0.05$ also agreed well with the earlier study, though H was somewhat larger than before, probably because it was determined by fitting the equation

$$w(l) = w_{\mathrm{sat}}\{1 - \exp[-(l/l_{\mathrm{c}})^H]\} \tag{23}$$

to the complete set of $w(l)$ data, rather than simply fitting a straight line to the data for $l \ll l_{\mathrm{c}}$. The latter method is much more subjective than using equation (23) because it requires an estimate of the cut-off above which $l \ll l_{\mathrm{c}}$ is no longer true.

Figure 11 shows w_{sat} as a function of l_c (both determined by fitting equation (23) to $w(l)$ data) for the edge and centre of Cu films electrodeposited on microelectrodes. Data from both the edge and the centre lie on the same straight line on the logarithmic plot. From equation (19), $w_{\mathrm{sat}} = a\, l_{\mathrm{c}}{}^{\alpha}$, where a is a constant. Hence not only the roughness exponent α but also the pre-factor a is the same at the centre and the edge. The former is expected if the scaling

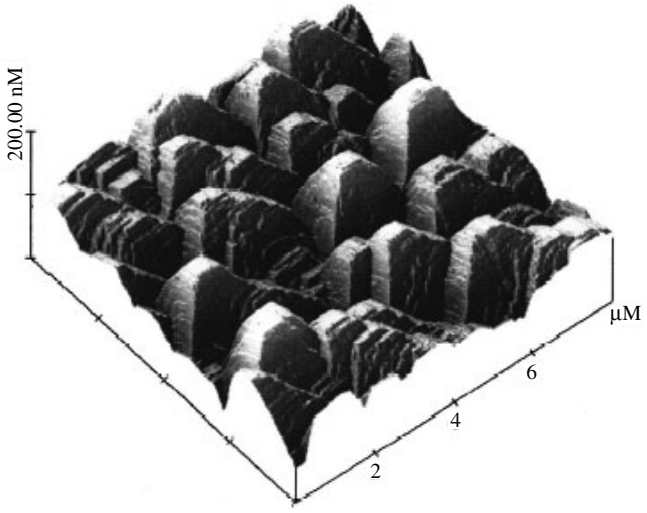

Figure 12. AFM image of a $t = 0.55$ μm Cu film electrodeposited from a 0.2 M $CuSO_4$/1.0 M H_2SO_4/1 mM HCl electrolyte on Cu(100). Reproduced by permission of The Electrochemical Society, Inc. from [8].

exponents H, β and β_{loc} are the same in both regions, but the latter is a non-trivial result. Note that plots like figure 11 immediately reveal anomalous scaling ($\alpha \neq H$) without requiring knowledge of the film thickness t, which is a particular advantage in cases such as deposition on a microelectrode where t varies across the film.

Wu and Barkey studied Cu electrodeposition on single-crystal Cu(100) [8]. They used a 0.2 M $CuSO_4$/1.0 M H_2SO_4 electrolyte containing a controlled quantity 1.0 mM of Cl^- ions, and their deposition current was applied in 1 s pulses, with 9 s off-time (zero applied current). Pulse electrodeposition is an attractive process because it allows higher instantaneous current densities, higher overpotentials and a finer-grained deposit without excessive depletion of the electrolyte close to the surface and corresponding diffusional instabilities. It does, however, complicate any analysis of the results in terms of j/j_{DL}. Perhaps the most interesting aspect of their work was that the change in substrate led to a very different film morphology. This is illustrated by figure 12, which shows an AFM image of a $t = 0.55$ μm Cu film, and should be compared with figure 10(a). A Cl^- adlayer is known to stabilize $\langle 100 \rangle$ steps on the Cu(100) surface and thereby give rise to pyramidal features [5–7]. Wu and Barkey therefore analysed their results both by calculating $w(l, t)$ and by a template matching process, finding that the lateral size of the pyramids increased with t, though not according to a power law. Their aspect ratio (ratio of height to base radius) also increased with t. This is a very interesting experimental system, and more work on the morphology evolution would be worthwhile.

Schwarzacher and Huo studied the dynamic scaling of Cu films electrodeposited from alkaline 0.18 M $CuSO_4$/0.25 M $K_4P_2O_7$ on Au (25 nm)/Ti(5 nm)/glass substrates [51]. The films grown from this electrolyte consisted of relatively large columnar grains, unlike those grown from acid sulfate electrolytes [49], which were nanocrystalline. The columnar microstructure resulted in l_c remaining nearly constant ($\beta \approx 0$) although w_{sat} increased rapidly: $\beta + \beta_{\mathrm{loc}} = 0.78 \pm 0.02$. Qualitatively similar behaviour was observed for sputtered columnar films [52].

Otero *et al* [53] studied Cu electrodeposition from a CuCN 0.8 M/KCN 2.0 M pH = 12 electrolyte in which the Cu is highly complexed, i.e. the Cu and cyanide ions form complexes

according to

$$Cu^{+} + 2CN^{-} \rightarrow Cu(CN)_2^{-}. \tag{24}$$

In this system also, w_{sat} increased with t according to a power law, consistent with equations (13*b*) or (18*b*), and $\beta + \beta_{loc} \geqslant 0.5$ was attributed to the diffusional instability. The authors measured w_{sat} for films of constant thickness t as a function of the current density j at which they were deposited, and noted that $w_{sat}(j)$ went through a maximum, so that for large j w_{sat} actually decreased with increasing j. They attributed this observation to the greater hydrogen evolution at higher j (Cu electrodeposition took place at more negative potentials than e.g. in acid sulfate electrolytes, because of the complexing with cyanide (equation (24))), which would stir the electrolyte and reduce the influence of the diffusional instability. If hydrogen evolution takes place preferentially at peaks and Cu deposition is suppressed there, that would also reduce w_{sat}. In this case hydrogen would be acting like an additive (section 3.3). The authors showed w_{sat} could also be reduced dramatically by the use of 1 mM Na_2SeO_3 and 1 g l^{-1} Na didodecylphosphate as additives. The influence of organic additives on kinetic roughening will be discussed in the next section.

6.2. Cu electrodeposition from electrolytes containing organic additives

Gewirth and co-workers applied scaling analysis to AFM data from Cu films electrodeposited from an acid sulfate electrolyte (0.05 M $CuSO_4$/0.5 M H_2SO_4) on (111) textured Au substrates with either no additive, 100 μM benzotriazole (BTA) or 100 μM thiourea [10]. Although their value of $H \approx 0.9$ for the additive-free electrolyte is consistent with the values reported by other workers [48–50], their value for the exponent describing the growth of l_c, $1/z \approx 1/8$ is significantly smaller. This could be because, unlike other studies, they eliminated trace Cl^- from their electrolyte, for example, by using a Hg/Hg_2SO_4/saturated K_2SO_4 reference electrode rather than the more common Hg/Hg_2Cl_2/saturated KCl (saturated calomel). For the electrolytes with organic additives, $1/z \approx 1/2$. For the range of film thickness t measured, l_c was larger in the absence of additives despite the smaller $1/z$. The saturation roughness with and without organic additives followed a power law consistent with equation (13*b*) or (18*b*), with $\beta + \beta_{loc}$ larger for the former but, for the range of t studied, w_{sat} again significantly greater for the latter.

The authors also applied spectral analysis to their data, using an equation of the form

$$c(\mathbf{q}) = \Omega \frac{\exp(2\sum A_n |\mathbf{q}|^n t) - 1}{\sum A_n |\mathbf{q}|^n} \tag{25}$$

where Ω is the volume of a growth unit, n an integer and A_n an associated constant, to fit $c(\mathbf{q})$, the Fourier transform of the autocovariance function

$$C(|\mathbf{l}|) = \langle h(\mathbf{r}+\mathbf{l})\, h(\mathbf{r})\rangle - \langle h(\mathbf{r})\rangle^2 . \tag{26}$$

Although equation (25) is apparently inconsistent with equations (13), it nevertheless also gave a good fit to the data, reinforcing the point that caution is needed when analysing AFM data, for which the range of l is necessarily limited. There is an excellent discussion of both scaling and spectral analysis in [54].

Gewirth and co-workers subsequently studied the influence of BTA and a series of systematically substituted BTA molecules on the kinetic roughening of electrodeposited Cu [55] and concluded that the reason films grown in the presence of BTA have lower w_{sat} and smaller l_c (i.e. are smoother and finer) than when no additive is present is that a polymeric Cu(I)BTA complex forms. This inhibits Cu diffusion, and, together with the passivation of growing nuclei by BTA, favours large numbers of small nuclei. Additive was consumed during

deposition, and beyond a critical $t = t_c$, which depended on the additive concentration, small numbers of large features formed, presumably where the local additive coverage was lowest. The associated sudden increase in w_{sat} also meant that equations (13*b*)/(18*b*) ceased to apply.

Vázquez *et al* also studied Cu electrodeposition from an acid sulfate electrolyte in the presence of different quantities of a thiourea derivative (1,3-diethyl-2-thiourea), and subsequently compared the electrodeposition of Cu in the presence and absence of the thiourea [56, 57]. The Edwards–Wilkinson model appeared to describe their data well, but this interpretation mainly relies on fitting $w(l)$ data close to $l = l_c$ and might therefore be open to question. As in the later work of Gewirth and co-workers on BTA [55], they found that beyond a critical t_c, which depended on the additive concentration, there was a rapid increase in w_{sat} accompanied by the formation of a small number of large features. They interpret the role of the additive as suppressing growth at protrusions to which it adsorbs preferentially. If the additive coverage is high everywhere, then this mechanism cannot operate, and the same group presented experimental evidence that this is indeed the case [58], though alternative explanations of brightening, such as the CEAC model (section 4) also predict that too high an additive coverage can lead to unstable growth.

In addition to their work in the absence of organic additives, Wu and Barkey studied Cu electrodeposition on Cu(100) from 0.2 M $CuSO_4$/1.0 M H_2SO_4/1.0 mM Cl^- in the presence of 100 μM BTA or 100 μM 3-mercaptopropane sulfonic acid (MPSA) [8]. The scaling equations (13)/(18) did not describe the data for MPSA very well, but for BTA they found clear evidence of anomalous scaling, with $1/z \approx 0.2$ but a very large values of $\beta_{loc} = 0.9$. Their template matching procedure showed that this behaviour was due to the feature aspect ratio increasing almost linearly with t.

Hasan *et al* also found evidence of anomalous scaling for Cu films deposited from electrolytes with a significant organic component [59]. Theirs was the first study of the kinetic roughening of films prepared by electroless deposition. Electroless deposition differs from conventional electrodeposition chiefly in that the electrons required to reduce metal ions to metal atoms are generated by a local electrochemical reaction at the substrate rather than supplied by an external circuit. Since deposition on a catalytically active substrate takes place on immersion in the electrolyte and electrical contact is not required, electroless deposition is very convenient and has found widespread use.

The electrolyte used in this study contained 0.04 M $CuSO_4$, 0.08 M EDTA (ethylenediaminetetraacetic acid), 0.004–0.24 M HCHO (formaldehyde) and 0.0004 M 2,2′-bipyridyl as stabilizer, with pH $\approx$ 12 adjusted by the addition of KOH. The electrolyte temperature was 65 °C. HCHO donates electrons to the neutral substrate (equation (27)), which then reduce Cu^{2+} ions (equation (28)). The latter are complexed with EDTA to increase the stability of the electrolyte further.

$$2\,HCHO + 4\,OH^- \rightarrow 2\,HCOO^- + 2\,H_2O + H_2 + 2e^-. \tag{27}$$

$$CuEDTA^{2-} + 2e^- \rightarrow Cu^0 + EDTA^{4-}_{ADS}. \tag{28}$$

The authors were able to change the deposition rate by a factor of four through varying the HCHO concentration [HCHO]. As was the case for Cu electrodeposition from organic additive-free acid sulfate electolytes [49], both $H = 0.74 \pm 0.03$ and $\beta = 0.28 \pm 0.03$ remained constant, while β_{loc} increased from 0.17 ± 0.03 to 0.31 ± 0.03 with increasing [HCHO], though it decreased again to 0.25 ± 0.03 at the highest HCHO concentration. Since Cu deposition goes from being kinetically controlled to control by Cu^{2+} diffusion as [HCHO] increases, the corresponding increase in β_{loc} for this system could also be due to the diffusional instability. The maximum value of $\beta + \beta_{loc}$ was significantly less than for electrodeposition

from the organic additive-free electrolyte, however, suggesting that adsorbed HCHO, EDTA and/or 2,2′-bipyridyl stabilize the growth.

6.3. Electrodeposition of other metals and alloys

The kinetic roughening of electrodeposited Ni films has also been studied intensively. Morales *et al* used STM to measure films grown on β-brass substrates from a Watt bath (300 g l^{-1} $NiSO_4$, 50 g l^{-1} $NiCl_2$, 50 g l^{-1} H_3BO_3) using a wide range of current densities [60]. They made the point that since Ni deposition takes place at potentials sufficiently negative for hydrogen evolution, adsorbed hydrogen can act as an additive and have a strong influence on the morphology evolution.

Saitou *et al* [61, 62] used scaling analysis to compare films prepared on indium tin oxide (ITO) coated glass substrates from an unstirred electrolyte (600 g l^{-1} $Ni(NH_2SO_3)_2$, 5 g l^{-1} $NiCl_2$, 40 g l^{-1} H_3BO_3) by continuous and pulse electrodeposition at the same average current density (2 mA cm^{-2}). They measured $\beta + \beta_{loc}$ as 0.78 ± 0.03 and 0.65 ± 0.02 for continuous and pulse deposition respectively. The large values of $\beta + \beta_{loc}$ suggested anomalous scaling, as did the observation that $G(l, t)$ was a function of t even for $l \ll l_c$. Saitou confirmed the existence of anomalous scaling in a later publication [63]. Since the average current density in these experiments was low, the anomalous scaling is unlikely to be caused by the diffusional instability.

These authors took particular care to measure H, using Hurst's re-scaled range analysis [1] as well as fitting the power spectrum of the surface by a power law [64]. The result was that within error $H = 1$, i.e. the surface is best described as a series of smooth mounds. Saitou *et al* are probably correct to claim that many of the values of H in the literature are too low (see section 7).

Saitou and co-workers also showed that the kinetic roughening of Ni electrodeposited from the same electrolyte but on single-crystal Ni(100) and at very low current densities (0.1 mA cm^{-2}) was quite different to that studied earlier on ITO coated glass substrates. In the early stages of growth, flat topped islands formed, and the scaling was normal, whereas in the later stages the surfaces of the islands became rough and anomalous scaling was observed [65].

In addition to Ni, Saitou *et al* have studied the kinetic roughening of Ge films electrodeposited from an electrolyte containing 5% $GeCl_4$ by volume in propylene glycol [66]. The current efficiency for this process was very low, only 1%. Beyond a certain t the roughness actually decreased, as gaps between mounds were filled, so $w(l, t)$ did not follow the dynamic scaling laws, equations (13) or (18). A similar decrease in $w(l, t)$ has been reported for Co films electrodeposited on Si [67]. Vela *et al* have also studied the kinetic roughening of a non-metal, films of electrodeposited polymer (polyaniline) [68]. Their results are interesting, because the different power law exponents β(I) and β(II) that they measured at different length scales l could correspond to β_{loc} and β, and indicate anomalous scaling.

Foster *et al* recently studied the kinetic roughening of Ag electrodeposited on an evaporated Ag surface from ammonium and sodium thiosulfate electrolytes (0.1 M AgBr, 0.20 M $(NH_4)_2SO_3$, 0.25 M $(NH_4)_2S_2O_3$, or 0.1 M AgBr, 0.2 M Na_2SO_3, 0.25 M $Na_2S_2O_3$) [69]. Although their data have quite a lot of scatter, there is evidence for anomalous scaling, with relatively small β, at least for deposition from the sodium thiosulfate electrolyte. Although $\beta + \beta_{loc}$ was larger for the sodium than the ammonium thiosulfate electrolyte, for the range of t studied, w_{sat} was significantly greater for the latter.

The same group also studied Ag electrodeposition from a similar electrolyte but using pulse reverse electrodeposition, whereby every 5 min of deposition at 0.8 mA cm^{-2} would be followed by 2.5 min dissolution at the same current density [70]. During the reverse pulse,

diffusion and hence dissolution should be more rapid from protrusions, resulting in a smoother film. The authors were able to show that w_{sat} depended on the number of cycles, which is proportional to the thickness t, as a power law, consistent with equations (13b)/(18b).

Relatively few studies have addressed the kinetic roughening of alloy films. Ebothé and Vilain have studied the morphology of Fe–Co and Ni–Co films of fixed t deposited from sulfate electrolytes as a function of the composition and deposition current [71]. They found that for both systems the pure metals have substantially greater w_{sat} than the alloys. They also found that w_{sat} goes through a minimum as the deposition current j is increased for the films containing Co, but not for pure Fe or Ni films, and were able to correlate this minimum with changes in the film texture. For example, the minimum in w_{sat} as a function of j for pure Co could be attributed to a transition between face-centred cubic (fcc) and hexagonal close-packed (hcp) structures, with the former predominant at low growth velocities.

Kurowski *et al* have investigated the kinetic roughening of electrodeposited Ni–P films [72]. This system is an interesting one because alloys containing more than ∼20% P are amorphous [73]. The authors measured $H = 1.07 \pm 0.05$ and $\beta = 0.28 \pm 0.05$. They did not report anomalous dynamic scaling, though their published $w(l, t)$ data suggest it.

7. Conclusions

There is now considerable experimental evidence for power law behaviour in the kinetic roughening of electrodeposited thin films, and it is clear that dynamic scaling, particularly anomalous scaling, provides a convenient description of the phenomenon. Once the scaling exponents H, β and β_{loc} have been determined for a system, together with the constants of proportionality in equations (18a) and (18b), the roughness of a film of any thickness t, on any length scale l, may be calculated. This is likely to prove of practical importance in electroplating. It is especially interesting that H and β remain fixed for a wide range of deposition conditions, while β_{loc} is a function of j/j_l. Despite significant progress, however, major experimental and theoretical challenges remain.

In general, since the range of accessible l is limited by the number of image pixels, and the cross-over region from power law behaviour (equations (13a)/(18a)) to saturation (equations (13b)/(18b)) is often broad, it is very easy to introduce systematic errors in the scaling analysis of data from AFM. Consequently, the values of H in the experimental literature measured from $w(l)$ data should be treated with caution. For example, the fact that H calculated from $w(l)$ and $G_2(l)$ by Cecchini *et al* [50] disagreed by more than the quoted experimental error reinforces this point, with the latter likely to be more accurate because it is not affected by artefacts introduced due to the discrete nature of the surface sampling. Similar problems affect the determination of l_c from $w(l)$ data, but, provided the same method of establishing l_c is used consistently, reported values of $1/z$ should be reasonably reliable. There should also be relatively few problems with reported values of $\beta + \beta_{loc}$.

While important, H and l_c clearly do not provide a complete description of the surface. Additional information is present in the complete $w(l)$ or $G(l)$. Of course, care must be taken to distinguish between systematic correlations that appear when averaging over many regions of the same surface, and random correlations. There are also too few studies that have tested for multi-affine scaling. Ideally, authors should calculate $w_q(l) = \sqrt[q]{\langle |h - \langle h \rangle|^q \rangle}$ and $G_q(l)$ (section 5.1) for several values of q. Note, however, that even in the case of multi-affine scaling, or a periodic surface, $H\,(=H_2)$ and l_c remain meaningful quantities (though care must clearly be taken over their interpretation).

Again, the range of t measured experimentally is often limited, usually because the surface rapidly becomes too rough to measure by SPM, and tip artefacts appear. Future progress will

probably require the combination of scanning probe microscopy and other forms of surface profiling to cover a greater range of (l, t). This would allow an answer to questions such as whether the anomalous scaling observed for Cu electrodeposition from organic additive-free electrolytes [49] is actually only transient, as predicted by some theoretical studies [39].

Progress is also needed with modelling the kinetic roughening of electrodeposited films. The agreement between experimentally determined scaling exponents and the predictions of simple models is generally extremely poor. This is not surprising, since such models do not take either the non-local nature of electrodeposition or the film and substrate microstructure into account. The latter is clearly important, because highly polycrystalline Cu films in which the crystallite size is significantly less than l_c [49] have a completely different morphology to films deposited from a similar electrolyte on Cu(100) [8]. Alkire and co-workers have carried out some multi-scale simulations of Cu electrodeposition, which could prove to be a promising approach, but so far the agreement with experiment is still poor [74].

Further studies will be needed to understand the origins of the constants of proportionality in the scaling equations (13) and (18). They will most probably depend on the film microstructure, which in turn depends on parameters ranging from the overpotential η to the anion species present in the electrolyte, and may be heavily influenced by the initial nucleation stage. Being able to predict these constants would have great practical benefits. Besides the continuous deposition of single metals on smooth substrates, understanding pulse deposition, pulse reverse deposition, alloy deposition and deposition on rough substrates all present interesting problems.

Finally, even though dynamic scaling describes the kinetic roughening of a wide variety of electrodeposited films, it does not apply to all systems. For example, for systems with organic additives, the roughness amplitude may remain nearly constant over a wide range of t. Such systems will also attract further interest.

References

[1] Meakin P 1998 *Fractals, Scaling and Growth far From Equilibrium* (Cambridge: Cambridge University Press)
[2] Krug J 1997 *Adv. Phys.* **46** 139
[3] Andricacos P C 1999 *Interface* **8** 32
[4] Mullins W W and Sekerka R F 1964 *J. Appl. Phys.* **35** 444
[5] Vogt M R, Möller F A, Schilz C M, Magnussen O M and Behm R J 1996 *Surf. Sci.* **367** L33–41
[6] Vogt M R, Lachenwitzer A, Magnussen O M and Behm R J 1998 *Surf. Sci.* **399** 49
[7] Damjanovic A, Paunovic M and Bockris J O'M 1965 *J. Electroanal. Chem.* **9** 93
[8] Wu A and Barkey D P 2003 *J. Electrochem. Soc.* **150** C533
[9] Franklin T C 1987 *Surf. Coat. Technol.* **30** 415
[10] Schmidt W U, Alkire R C and Gewirth A A 1996 *J. Electrochem. Soc.* **143** 3122
[11] Madore C, Matlosz M and Landolt D 1996 *J. Electrochem. Soc.* **143** 3927
[12] Moffat T P, Wheeler D, Huber W H and Josell D 2001 *Electrochem. Solid State Lett.* **4** C26
[13] Josell D, Wheeler D, Huber W H and Moffat T P 2001 *Phys. Rev. Lett.* **87** 016102
[14] Aogaki R, Kitazawa K, Kose Y and Fueki K 1980 *Electrochim. Acta* **25** 965
[15] Aogaki R and Makino T 1981 *Electrochim. Acta* **26** 1509
[16] Aogaki R and Makino T 1984 *J. Electrochem. Soc.* **131** 40
[17] Wolf D E and Villain J 1990 *Europhys. Lett.* **13** 389
[18] Barkey D P, Muller R H and Tobias C W 1989 *J. Electrochem. Soc.* **136** 2207
[19] Chen C-P and Jorne J 1991 *J. Electrochem. Soc.* **138** 3305
[20] Haataja M, Srolovitz D J and Bocarsly A B 2003 *J. Electrochem. Soc.* **150** C699
[21] Haataja M, Srolovitz D J and Bocarsly A B 2003 *J. Electrochem. Soc.* **150** C708
[22] McFadden G B, Coriell S R, Moffat T P, Josell D, Wheeler D, Schwarzacher W and Mallett J 2003 *J. Electrochem. Soc.* **150** C591
[23] Aogaki R and Makino T 1984 *J. Electrochem. Soc.* **131** 46
[24] Family F and Vicsek T 1985 *J. Phys. A: Math. Gen.* **18** L75

[25] Kardar M, Parisi G and Zhang Y-C 1986 *Phys. Rev. Lett.* **56** 889
[26] He Y-L, Yang H-N, Lu T-M and Wang G-C 1992 *Phys. Rev. Lett.* **69** 3770
[27] Palasantzas G and Krim J 1994 *Phys. Rev. Lett.* **73** 3564
[28] Barabási A-L and Vicsek T 1991 *Phys. Rev.* A **44** 2730
[29] Schroeder M, Siegert M, Wolf D E, Shore J D and Plischke M 1993 *Europhys. Lett.* **24** 563
[30] Das Sarma S, Ghaisas S V and Kim J M 1994 *Phys. Rev.* E **49** 122
[31] López J M 1999 *Phys. Rev. Lett.* **83** 4594
[32] Palasantzas G 1997 *Phys. Rev.* E **56** 1254
[33] Brú A, Pastor J M, Fernaud I, Brú I, Melle S and Berenguer C 1998 *Phys. Rev. Lett.* **81** 4008
[34] López J M and Schmittbuhl J 1998 *Phys. Rev.* E **57** 6405
[35] Morel S, Schmittbuhl J, López J M and Valentin G 1998 *Phys. Rev.* E **58** 6999
[36] Zhao Y-P, Fortin J B, Bonvallet G, Wang G-C and Lu T-M 2000 *Phys. Rev. Lett.* **85** 3229
[37] Sneppen K, Krug J, Jensen M H, Jayaprakash C and Bohr T 1992 *Phys. Rev.* A **46** R7351
[38] Edwards S F and Wilkinson D R 1982 *Proc. R. Soc.* A **381** 17
[39] Cuerno R and Castro M 2001 *Phys. Rev. Lett.* **87** 236103
[40] Buceta J, Pastor J M, Rubio M A and de la Rubia F J 1997 *Phys. Lett.* A **235** 464
[41] Buceta J, Pastor J M, Rubio M A and de la Rubia F J 1998 *Physica* D **113** 166
[42] Sánchez A, Bernal M J and Riveiro J M 1994 *Phys. Rev.* E **50** R2427
[43] Castro M, Cuerno R, Sánchez A and Domínguez-Adame F 1998 *Phys. Rev.* E **57** R2491
[44] Castro M, Cuerno R, Sánchez A and Domínguez-Adame F 2000 *Phys. Rev.* E **62** 161
[45] de Leon P F J, Albano E V, Salvarezza R C and Solari H G 2002 *Phys. Rev.* E **66** 042601
[46] Kahanda G L M K S, Zou X-Q, Farrell R and Wong P-Z 1992 *Phys. Rev. Lett.* **68** 3741
[47] Pastor J M and Rubio M A 1996 *Physica* D **96** 384
[48] Iwamoto A, Yoshinobu T and Iwasaki H 1994 *Phys. Rev. Lett.* **72** 4025
[49] Huo S and Schwarzacher W 2001 *Phys. Rev. Lett.* **86** 256
[50] Cecchini R, Mallett J J and Schwarzacher W 2003 *Electrochem. Solid State. Lett.* **6** C103
[51] Schwarzacher W and Huo S 2003 *Phys. Rev. Lett.* **91** 119601
[52] Santamaria J, Gómez M E, Vicent J L, Krishnan K M and Schuller I K 2002 *Phys. Rev. Lett.* **89** 190601
[53] Otero T F, Rodríguez-Jiménez J L, Martín H, Carro P, Krijer S M and Hernández-Creus A 2000 *J. Electrochem. Soc.* **147** 4546
[54] Tong W M and Williams R S 1994 *Annu. Rev. Phys. Chem.* **45** 401
[55] Leung T Y B, Kang M, Corry B F and Gewirth A A 2000 *J. Electrochem. Soc.* **147** 3326
[56] Vázquez L, Salvarezza R C and Arvia A J 1997 *Phys. Rev. Lett.* **79** 709
[57] Mendez S, Andreasen G, Schilardi P, Figueroa M, Vázquez L, Salvarezza R C and Arvia A J 1998 *Langmuir* **14** 2515
[58] Schilardi P L, Azzaroni O and Salvarezza R C 2000 *Phys. Rev.* B **62** 13098
[59] Hasan N M, Mallett J J, dos Santos Filho S G, Pasa A A and Schwarzacher W 2003 *Phys. Rev.* B **67** 081401(R)
[60] Morales J, Krijer S M, Esparza P, González S, Vázquez L, Salvarezza R C and Arvia A J 1996 *Langmuir* **12** 1068
[61] Saitou M, Makabe A and Tomoyose T 2000 *Surf. Sci.* **459** L462
[62] Saitou M, Oshikawa W, Mori M and Makabe A 2001 *J. Electrochem. Soc.* **148** C780
[63] Saitou M 2002 *Phys. Rev.* B **66** 073416
[64] Saitou M, Oshikawa W and Makabe A 2002 *J. Phys. Chem. Solids* **63** 1685
[65] Saitou M, Hamaguchi K and Oshikawa W 2003 *J. Electrochem. Soc.* **150** C99
[66] Saitou M, Sakae K and Oshikawa W 2002 *Surf. Coat. Technol.* **162** 101
[67] Munford M L, Sartorelli M L, Seligman L and Pasa A A 2002 *J. Electrochem. Soc.* **149** C274
[68] Vela M E, Andreasen G, Salvarezza R C and Arvia A J 1996 *J. Chem. Soc. Faraday Trans.* **92** 4093
[69] Foster D G, Shapir Y and Jorne J 2003 *J. Electrochem. Soc.* **150** C375
[70] Shapir Y, Raychaudhuri S, Foster D G and Jorne J 2000 *Phys. Rev. Lett.* **84** 3029
[71] Ebothé J and Vilain S 1999 *J. Phys. D: Appl. Phys.* **32** 2342
[72] Kurowski A, Schultze J W and Staikov G 2002 *Electrochem. Commun.* **4** 565
[73] Schlesinger M and Paunovic M (ed) 2000 *Modern Electroplating* 4th edn (New York: Wiley)
[74] Pricer T J, Kushner M J and Alkire R C 2002 *J. Electrochem. Soc.* **149** C396